JOURNAL OF SOLID STATE CHEMISTRY 93, 163–172 (1991)

Lanthanum Substitution for Barium in $YBa_2Cu_3O_{9-\delta}$

P. KAREN, H. FJELLVÅG AND A. KJEKSHUS

Department of Chemistry, University of Oslo, Blindern, N-0315 Oslo 3, Norway

AND A. F. ANDRESEN†

Institute for Energy Technology, N-2007 Kjeller, Norway

Received December 4, 1990; in revised form March 8, 1991

A detailed mapping is given for the existence range of the $Y(Ba_{1-y}La_y)_2Cu_3O_{9-\delta}$ solid solution phase with respect to y and δ. The findings are presented in the tetrahedral phase diagram of the Y(O)–Ba(O)–La(O)–Cu(O) system. All samples were carefully prepared by citrate methods and gettering techniques giving high resolution in the degree of substitution y and oxygen content $9-\delta$. The upper substitution limit of $y = 0.36(2)$ can notably be exceeded if one at the same time allows substitution of Y by La, viz., by extending the phase region to include $(Y_{1-x}La_x)(Ba_{1-y}La_y)_2Cu_3O_{9-\delta}$. For $Y(Ba_{1-y}La_y)_2Cu_3O_{9-\delta}$, the lower limit for the oxygen content $9-\delta$ increases strongly with y, from 6.00(3) for $y = 0.00$ to, say, 6.45(3) for $y = 0.20$. The upper limit is approximately given as $9-\delta = 6.95 + y_{O,T}$ [$0.00 < y < 0.36(2)$], i.e., the maximum formal Cu valency remains constant. Hence, oxygen contents well above seven per formula can be achieved, and for such samples the crystal symmetry eventually turns tetragonal, as seen by X-ray and neutron diffraction. A three-dimensional representation of the degree of orthorhombic distortion together with the parameters y and $9-\delta$ is made in the range where orthorhombic symmetry is adopted. For fully oxygenated samples (saturation at 340°C; $P_{O_2} = 100$ kPa; Cu valence constant: 2.30(1) according to iodometry), the symmetry change occurs at $y_{O,T} = 0.140(5)$; $9-\delta = 7.10$. At the somewhat lower oxygen contents between 6.9 and 7.0, the domain of the orthorhombic state extends, e.g, to $y_{O,T} = 0.160(5)$ for $9-\delta = 6.98$. An interesting consequence of this is that oxygen rich samples from the intermediate composition interval $0.14 < y < 0.16$ undergo the phase transition sequence tetragonal to orthorhombic to tetragonal upon thermal removal of oxygen.

Introduction

Since the discovery of the high-T_c superconducting oxides (*1*), significant efforts have been devoted to elucidate the structural and chemical conditions for this phenomenon. A mixed valence state, adhered to a network of key blocks (e.g., to the $[Cu_3O_{9-\delta}^{7-}]_n$ anionic net in the structure of $YBa_2Cu_3O_{9-\delta}$), seems to be one prerequisite. The mixed valence state can readily be manipulated by controlling the amount of oxygen vacancies. In $YBa_2Cu_3O_{9-\delta}$, the concentration of oxygen vacancies is controlled via a pseudochemical solid–gas equilibrium (*2*). By changing the partial pressure of O_2, δ can be varied from ~2 to ~3. The increase in δ results in a smooth, continuous

† Deceased.

0022-4596/91 $3.00

structural change from orthorhombic to tetragonal symmetry. During this process, the Cu coordination square situated parallel to the potential fourfold axis is being depleted of oxygens to ultimately become a linear O–Cu–O coordination (*3, 4*).

On the other hand, insertion of additional oxygen atoms into $YBa_2Cu_3O_{\sim 7}$ is also of high interest. Unfortunately, at high O_2 pressures, another phase, $YBa_2Cu_4O_8$ is stabilized (*5*). Alternatively, accommodation of peroxy-groups in the structure is considered (*6*). However, the most fruitful attempts (*7–18*) to accomplish a higher oxygen content are made by substituting Ba by another, higher valent element. As communicated earlier (*7*), lanthanum is the only trivalent element which (partially) substitutes for Ba in $YBa_2Cu_3O_{9-\delta}$ in a manner that leaves the Y site intact. This enables a direct comparison with the widely studied $YBa_2Cu_3O_{9-\delta}$ parent phase.

The present work reports on a comprehensive study by means of powder X-ray and neutron diffraction methods on the structural aspects of La for Ba substitution in well-characterized samples of $Y(Ba_{1-y}La_y)_2Cu_3O_{9-\delta}$. The study covers the entire homogeneity range with respect to oxygen content. Temperature-induced changes in the crystal structure between 8 and 1250 K are discussed.

Experimental

Synthesis. All samples were synthesized using the technique of liquid mixing of citrate gels, followed by preparation cycles involving homogenization, firing, and controlled oxidation. The samples were prepared using reagent grade or higher purity starting materials: $La(NO_3)_3 \cdot 6H_2O$, (Merck); Y_2O_3 (5*N*, Megon); $BaCO_3$ (Merck), $CuCO_3 \cdot Cu(OH)_2 \cdot 0.5H_2O$ (Riedel de Häen), and citric acid monohydrate (Fluka).

Dried yttrium oxide was dissolved in melted citric acid monohydrate, and stoichiometric amounts of dry $BaCO_3$, analyzed basic copper carbonate, and $La(NO_3)_3 \cdot 6H_2O$ were added to the solution together with water. The resulting clear citrate gel was dehydrated at 180°C in order to obtain solidified citrate. After milling and subsequent burning in air at 450°C, the obtained powder was pressed into pellets and fired at 910°C for 20 hr and at 340°C for 16 hr (intermediate cooling rate 120°C/hr) in a corundum boat placed inside a tube furnace. The furnace was continuously flushed with oxygen gas purified on CuO at 600°C and on KOH at ambient temperature. The rehomogenizations of the fired samples were performed in an ultrafine agate vibrational mill, the last one (usually the third) involved only coarse crushing in order to facilitate easy and full oxygen saturation.

Oxygen content control and analysis. The amount of (bonded) oxygen in the samples was varied by means of deoxidation by controlled amounts of Ti powder (100–150 μm fraction, Koch-Light Lab., Ltd.) in closed silica glass ampoule systems. The getter part of the ampoule was heated at 750°C for 48 hr, whereas the sample part was kept at 450°C. The sample part was finally annealed at 320°C for 24 hr to ensure homogeneous oxygen distribution throughout the sample. Minute reductions of the oxygen-saturated samples were accomplished without any getter, by simply varying the size of the evacuated ampoule. On the other hand, when an extensive oxygen removal was required, the samples were equilibrated with an excess of Cu/Cu_2O so that the degree of deoxidation was controlled by the temperature selection. The sample and the getter (activated Cu sponge, predeposited in the tube by a glow heat interaction of Cu powder with C_2H_5OH vapor) were heated 72 hr at 700 to 800°C, followed by slow cooling at 50°C/hr.

The oxygen content was determined iodometrically using the standard technique of

thiosulfate titrations of iodine oxidized from iodide solution by the sample as such in a first set, and by the HCl-prereduced sample in a second set. Finely milled samples and an Ar protection atmosphere were used in the first set of determinations. Addition of NH_4SCN and soluble starch immediately before the end point facilitated exact titrations in both cases. The reproducibility of the determination is ±0.005 in units of the formal oxidation state of copper, provided this is higher than two. For lower Cu-oxidation states, the estimated uncertainties may be up to ±0.03, and are stated in the text. The reproducibility of obtaining a certain Cu-oxidation state via the getter-reduction is generally poorer than these figures indicate.

Powder X-ray diffraction (PXD). All samples were characterized by PXD measurements using Guinier Hägg cameras, Cu$K\alpha_1$ radiation and Si as internal standard. High temperature PXD data were measured at temperatures between 20 and 1000°C using a Guinier Simon camera (Enraf–Nonius) and Mo$K\alpha_1$ radiation. The samples, placed in a rotating quartz capillary open to the atmosphere, were heated at a rate of 50°C/hr. The temperature was calibrated by simultaneous measurements of thermal expansion and melting point of Ag. Positions and integrated intensities of Bragg reflections were obtained from the films by means of a Nicolet L18 film scanner using the SCANPI program system (*19*). Unit cell parameters were deduced by least square refinements (*20*) including only unambiguously indexable lines.

Powder neutron diffraction (PND). The data were obtained using the two-axis diffractometer OPUS III at the JEEP II reactor, Kjeller. Monochromatized neutrons of wavelength 187.7 pm were used, and diffraction data were collected in steps of $\Delta 2\theta$ = 0.05° between 2θ = 5 and 100°. Least squares profile refinements were carried out according to the Rietveld method (*21*) using the Hewat version (*22*) of the program. The scattering lengths b_Y = 7.75, b_{Ba} = 5.25, b_{La} = 8.27, b_{Cu} = 7.718, and b_O = 5.805 fm were used (*23*). In the profile refinements one common isotropic temperature factor was adopted for the metal atoms, viz., $B = 39 \cdot 10^{-6}$ pm^{-2} ($B = 49 \cdot 10^{-6}$ pm^{-2} for the oxygen atoms), since the small number of reflections and the large number of structural variables do not justify introduction of individual or anisotropic thermal parameters.

Results

Homogeneity Region

The introduction of La into $YBa_2Cu_3O_{9-\delta}$ is a complex process, since both the Y and the Ba sites may be subjected to substitution (*24*), and $(Y_{1-x}La_x)(Ba_{1-y}La_y)_2Cu_3O_{9-\delta}$ is generally formed. The experimental results are summarized in the tetrahedral phase diagram in Fig. 1, where the relevant portion around the homogeneity region is drawn, including parallel results for the $(Y_{1-x}La_x)_2BaCuO_5$, $(Y,Ba,La)_2(Ba,La)CuO_5$, and $La_{2-x}Ba_{1+x}Cu_2O_y$ solid solutions. Other phases are taken from Refs. (*25–27*).

$Y(Ba_{1-y}La_y)_2Cu_3O_{9-\delta}$ represents one frontier of the homogeneity region. Phase pure samples (≥99.5%), according to this formula, are prepared up to a substitution level of y = 0.30 at P_{O_2} = 100 kPa. If higher substitutions (e.g., y = 0.40) are attempted, La starts to replace Y. Yttrium then emerges as $Y_2Cu_2O_5$. According to quantitative analyses based on PXD data for such two-phase samples, the limit of the La for Ba substitution in $Y(Ba_{1-y}La_y)_2Cu_3O_{9-\delta}$ is y = 0.36(2). For the nominal y = 0.40 substitution, $Y_{0.925}La_{0.075}(Ba_{0.62}La_{0.38})_2Cu_3O_{7.30}$ is formed instead, accompanied by 3.6 pseudo-atom% of $Y_2Cu_2O_5$. A y = 0.50 nominal substitution yields $Y_{0.67}La_{0.33}(Ba_{0.58}La_{0.42})_2Cu_3O_{7.31}$ together with 14 pseudo-atom% of $Y_2Cu_2O_5$.

For samples saturated in oxygen (P_{O_2} =

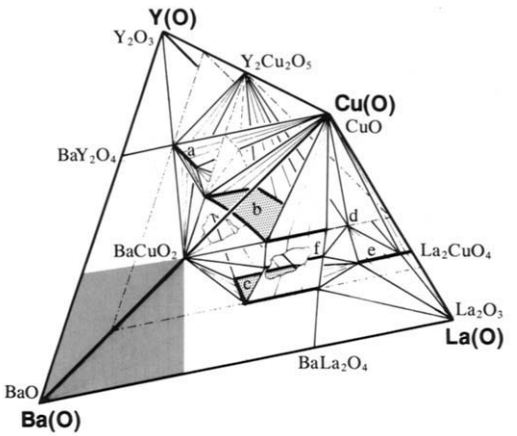

FIG. 1. Pseudoquaternary tetrahedral diagram of the La(O)–Y(O)–Ba(O)–Cu(O) system as observed for samples fired at 910°C and saturated in P_{O_2} = 100 kPa at 340°C. Phases from the BaO corner (shaded) are omitted. Phase labeling: a, orthorhombic $(Y_{1-x}La_x)_2BaCuO_5$; b, $Y_{1-x}La_x(Ba_{1-y}La_y)_2Cu_3O_{9-\delta}$; c, tetragonal $(Y,Ba,La)_2(Ba,La)CuO_5$; d, $BaLa_4Cu_5O_{13}$; e, $(La,Ba)_2CuO_4$; f, $La_{2-x}Ba_{1+x}Cu_2O_y$. Line distinctions: thick, solid solution frontiers; normal, tie lines; thin, solid solution tie lines; broken, pseudo-pseudoternary cuts, [LaCu(O)—YCu(O)—BaCu(O) and $La_3Cu(O)$—$Y_3Cu(O)$—$Ba_3Cu(O)$, both drawn as nontransparent]; dashed, intersections of three-phase walls with a cut plane.

100 kPa; 340°C), the obtained formal copper valency v_{Cu} is virtually constant, v_{Cu} = 2.30(1). This is reflected in a continuous rise of the oxygen content, since divalent Ba is being replaced by trivalent La. The formula for the oxygen-saturated solid solution phase may therefore be written as $Y(Ba_{1-y}La_y)_2Cu_3O_{6.95(2)+y}$.

The lowest formal valency of Cu, attainable upon oxygen removal, is significantly affected by the substitution. In the pure nonsubstituted $YBa_2Cu_3O_{9-\delta}$, a reduction of copper to v_{Cu} = 1.67, when $9 - \delta = 6.00$, can be reached (at 750°C and $P_{O_2} = 2 \times 10^{-5}$ Pa above Cu_2O/Cu), but such low oxidation states become unstable upon substitution. For y = 0.10 and 0.20, the lower limits of stability are v_{Cu} = 1.80(2) when $9 - \delta = 6.30(3)$, and v_{Cu} = 1.85(2) when $9 - \delta = 6.45(3)$, respectively. Any further removal of oxygen leads to the formation of impurities.

Structural Properties

1. *Formal Cu valency constant.* A smooth variation of the unit cell parameters of the *oxygen-saturated* $Y(Ba_{1-y}La_y)_2Cu_3O_{6.95(2)+y}$ phase and a transition from orthorhombic to tetragonal symmetry are observed upon increasing La content, as shown in Fig. 2. The response of the structure to the introduction of the smaller La atoms is rather anisotropic. The c axis contracts,

$$c = 3[389.50(5) - 19.5(4) \cdot y]$$

$$(\text{pm};\ 0.00 \le y \le 0.20),$$

whereas the remaining two cell edges change in a manner that makes their sum practically constant:

$$a + b = 2[385.13(9) + 1.5(7) \cdot y]$$

$$(\text{pm};\ 0.00 \le y \le 0.20).$$

However, the a/b ratio is significantly affected by the substitution, and the ortho-

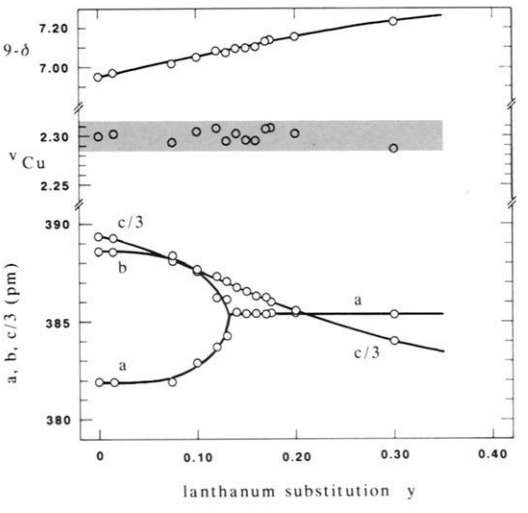

FIG. 2. Unit cell parameters at 300 K (size of symbols is at least five times the calculated standard deviations), formal Cu valency, v_{Cu}, and oxygen content, $9 - \delta$, as functions of La substitution in *oxygen-saturated* (P_{O_2} = 100 kPa, 340°C) $Y(Ba_{1-y}La_y)_2Cu_3O_{9-\delta}$.

rhombic distortion vanishes with increasing degree of substitution y. $Y(Ba_{1-y}La_y)_2Cu_3O_{6.95(2)+y}$ becomes tetragonal (as seen by room temperature PXD) for $y_{O,T} = 0.140(5)$.

When substitution levels above $y = 0.36(2)$ are attempted, the resulting partial replacement of Y (which accompanies the still progressing La for Ba substitution) is manifested as an increase in the unit cell parameters. The data and trends in Fig. 2 should be compared to $a = 385.65(3)$, $c = 1149.00(14)$ pm and $a = 385.86(7)$, $c = 1153.2(9)$ pm for $(Y_{0.925}La_{0.075})(Ba_{0.62}La_{0.38})_2Cu_3O_{7.30}$ and $(Y_{0.67}La_{0.33})(Ba_{0.58}La_{0.42})_2Cu_3O_{7.31}$, respectively. An annealing-persistent line-broadening is moreover observed in the PXD pattern of the latter sample, thereby indicating stress fields due to the size imbalance between the solute and the solvent atoms.

A slightly different course of the unit cell parameters is found after partial reduction of the oxygen-saturated samples. As an example, the variations in the unit cell parameters for $Y(Ba_{1-y}La_y)_2Cu_3O_{9-\delta}$ with formal copper valency $v_{Cu} = 2.27(1)$ and $v_{Cu} = 2.30(1)$ are compared in Fig. 3. It is realized that the orthorhombic distortion *decreases* when oxygen is removed from samples with oxygen content below $9 - \delta = 6.97(2)$. If oxygen is removed from samples with a higher oxygen content, the distortion *increases*, until the oxygen content reaches the value $9 - \delta = 6.97(2)$.

Structural parameters and occupation numbers for oxygen, as refined from low temperature PND data, for four $Y(Ba_{1-y}La_y)_2Cu_3O_{6.91(2)+y}$ samples (note the slightly reduced oxygen contents) are given in Table I. The refinements for all samples were carried out according to space group *Pmmm*, and the results obtained for $y = 0.150$ and 0.200 were compared with similar refinements according to space group *P4/mmm*. After considering the calculated standard deviations and possible systematic errors in both the PXD and PND data, it is concluded that $Y(Ba_{0.85}La_{0.15})_2Cu_3O_{7.06(2)}$ is tetragonal

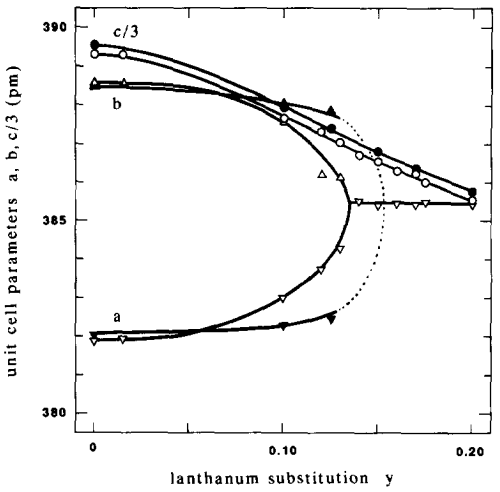

FIG. 3. Unit cell parameters at 300 K as a function of La substitution in $Y(Ba_{1-y}La_y)_2Cu_3O_{9-\delta}$ at constant formal Cu valency $v_{Cu} = 2.30(1)$, open symbols, and $v_{Cu} = 2.27(1)$, closed symbols. Size of symbols (a ▽, ▼; b △, ▲; $c/3$ ○, ●) is at least twice the calculated standard deviations. Note that ▽ and ▼ overlap for $y = 0.15$, 0.17 and 0.20.

at all temperatures between 8 and 300 K. From the oxygen occupation numbers, it is clearly seen that the additional oxygen, brought about by the aliovalent substitution in the amount of y per formula unit, enters the O(5) site at $\frac{1}{2}$, 0, 0. At the same time, a gradual redistribution of oxygen from the O(1) to the O(5) site occurs. As the substitution progresses, an equal occupancy of both positions is eventually reached and the structure turns tetragonal.

2. *Oxygen content constant.* Maintaining a constant oxygen content enables us to infer the structural effects of a sole replacement of Ba by La. The oxygen content corresponding to the highest orthorhombic distortion of the parent compound was chosen, and hence all substituted samples were reduced to $Y(Ba_{1-y}La_y)_2Cu_3O_{6.98(3)}$. As follows from Fig. 4, the degree of orthorhombic distortion remains rather high for $0.00 \leq y \leq 0.15$. The transition to tetragonal symmetry at room temperature occurs in this series at $y_{O,T} = 0.160(5)$, compared with

TABLE I

REFINED STRUCTURAL PARAMETERS OF $Y(Ba_{1-y}La_y)_2Cu_3O_{6.91(2)+y}$ AT 8 K

	Pmmm				*P4/mmm*		
	$y = 0.075$	$y = 0.100$	$y = 0.150$	Site	$y = 0.150$	$y = 0.200$	Site
$z_{Ba/La}$	0.1782(7)	0.1773(7)	0.1797(8)	2*t*	0.1788(8)	0.1817(9)	2*h*
$z_{Cu(2)}$	0.3589(5)	0.3577(4)	0.3557(6)	2*q*	0.3558(6)	0.3558(6)	2*g*
$z_{O(2)}$	0.1623(8)	0.1623(7)	0.1619(9)	2*q*	0.1628(9)	0.1604(11)	2*g*
$z_{O(3)}$	0.3812(8)	0.3803(8)	0.3775(9)	2*s*	0.3792(5)	0.3784(5)	4*i*
$z_{O(4)}$	0.3784(7)	0.3780(8)	0.3797(8)	2*r*			
$n_{O(1)}$	0.94(2)	0.90(2)	0.51(2)	1*e*	0.54(1)	0.56(2)	2*f*
$n_{O(5)}$	0.06(1)	0.11(1)	0.56(2)	1*b*			
a	381.0(1)	382.1(1)	384.4(1)		384.4(1)	384.4(1)	
b	387.6(1)	386.9(1)	384.0(1)				
c	1160.2(3)	1159.3(3)	1155.6(3)		1155.7(3)	1153.7(3)	

Note. Atomic coordinates *z*, oxygen occupancies *n*, and unit cell parameters (in pm, after correction for zero point of diffractometer; standard deviations estimated), as obtained by Rietveld refinements (R_N between 0.06 and 0.07) from PND data. *Y* at $\frac{1}{2}, \frac{1}{2}, \frac{1}{2}$ and Cu(1) at 0, 0, 0 are fixed by symmetry; occupancies of O(2), O(3), and O(4) constrained at 1.00.

$y_{O,T} = 0.140(5)$ for the oxygen-saturated samples (cf. Fig. 3). Actually, differences in oxygen content among samples investigated in various studies (*8, 9, 11, 12, 16, 17*) are most probably the reason for the reported wide span ($y_{O,T}$ ranging between 0.15 and 0.20) of critical concentrations. The highest values of $y_{O,T}$ correlate with unfavorable preparation conditions [e.g., with respect to temperature (*8, 9*) or time (*17*)] for achieving a high oxygen content. The unit cell parameter *c* of $Y(Ba_{1-y}La_y)_2Cu_3O_{6.98(3)}$ contracts linearly with increasing La content *y*,

$$c = 3[389.4(2) - 14(1) \cdot y]$$

$$(\text{pm};\ 0.00 \leq y \leq 0.20).$$

The contraction is smaller than for the corresponding, virtually oxygen-saturated $Y(Ba_{1-y}La_y)_2Cu_3O_{6.95(2)+y}$, in which the increased shielding between the two neighboring Ba/La site below and above the *ab* plane (originating from the higher oxygen occupancy) contributes to the contraction of *c*. No such distinction between the two series is observed for $(a + b)/2$, and

$$a + b = 2[385.1(1) + 1.5(7) \cdot y]$$

$$(\text{pm};\ 0.00 \leq y \leq 0.20).$$

3. *Lanthanum content constant.* The unit cell parameters for $Y(Ba_{1-y}La_y)_2Cu_3O_{9-\delta}$ are shown in Fig. 5 as functions of the oxygen content for $y = 0.00$, 0.10, 0.15, and 0.20. Since the parent compound ($y = 0.00$) has no homogeneity range with respect to the metal constituents under the chosen preparative conditions, its unit cell parameters depend entirely on the way and degree of oxygen accommodation in the structure. Both of these factors are strongly affected by the thermal treatment. Different thermal histories of samples (quenched, equilibrated) are reported (*28–32*) to give different unit cell parameters versus oxygen content relationships. In order to standardize the way of ordering of oxygen and vacancies, all samples discussed in this chapter were annealed for 24 hr at 320°C, after gettering at 600°C. The presented unit cell parameters are believed to reflect the oxygen arrangement in a reproducible and comparable manner.

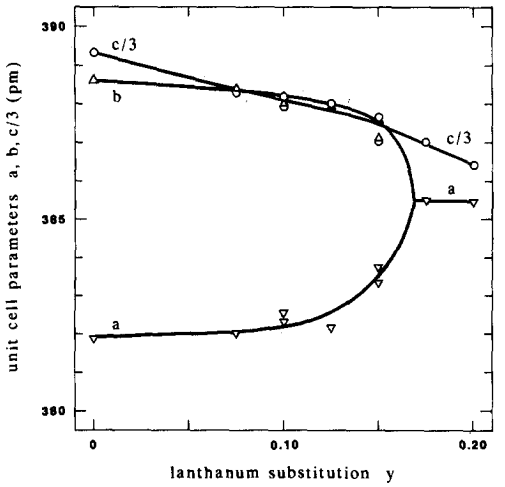

FIG. 4. Unit cell parameters at 300 K as a function of La substitution in $Y(Ba_{1-y}La_y)_2Cu_3O_{6.98(3)}$; note the constant oxygen content. (*a* ▽, *b* △, and *c*/3 ○; size of symbols is at least twice the calculated standard deviations.)

The removal of oxygen from the nonsubstituted $YBa_2Cu_3O_{9-\delta}$ phase leads to a diminishing orthorhombic distortion and finally to a transition to tetragonal symmetry when $9 - \delta = 6.25(5)$, at room temperature. The unit cell parameter *c* increases as the oxygen atoms are being removed from the coordination polyhedra around Cu(1), due to the increasing Ba–Ba repulsion. A slight change in the slope of the *c* versus oxygen content curve is found between oxygen contents 6.2 and 6.4. This change is smaller than the jump observed by Cava *et al.* (*29, 31*), probably due to differences in gettering and annealing temperatures. The curve for the quenched samples in Refs. (*28, 32*) is, on the other hand, quite smooth. The La substitution significantly diminishes the range in oxygen content where the structure is orthorhombic. For $y = 0.10$, the critical oxygen content rises to $9 - \delta = 6.60(5)$. However, for $y = 0.15$, two critical oxygen contents are observed, [$9 - \delta = 6.90(2)$ and $7.02(2)$], i.e., the structure is orthorhombic just over a small interval in oxygen content. For $y = 0.20$, the structure is tetragonal over the entire homogeneity range of oxygen content, i.e. $6.45 \leq 9 - \delta \leq 7.15$.

Temperature Induced Structural Effects

Due to the pseudochemical equilibrium between oxygen and vacancies in the solid, the structural characteristics at high temperatures will be affected by temperature-induced changes in the oxygen content, unless such changes are prevented by maintaining a proper equilibrium partial pressure of oxygen. This is usually not the case, and

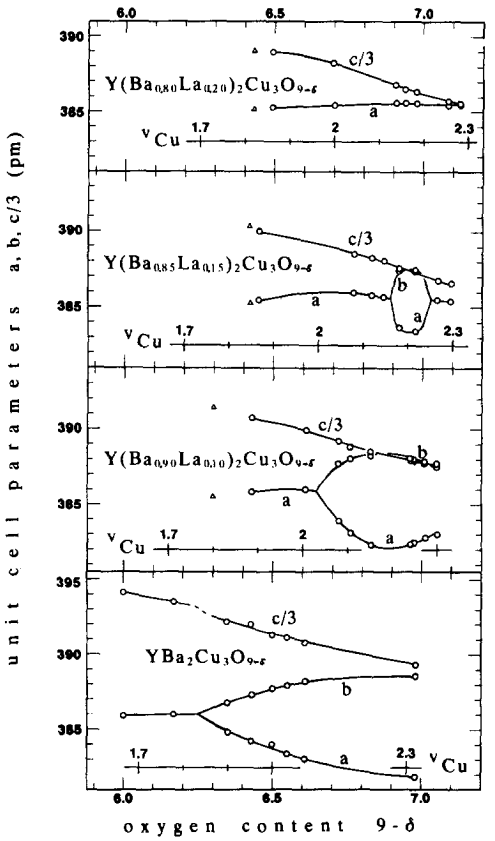

FIG. 5. Unit cell parameters at 300 K as a function of oxygen content in $Y(Ba_{1-y}La_y)_2Cu_3O_{9-\delta}$ for $y = 0.00, 0.10, 0.15$, and 0.20. Size of circles exceeds four times the calculated standard deviations; triangles denote first observation of impurities and refer to overall oxygen content.

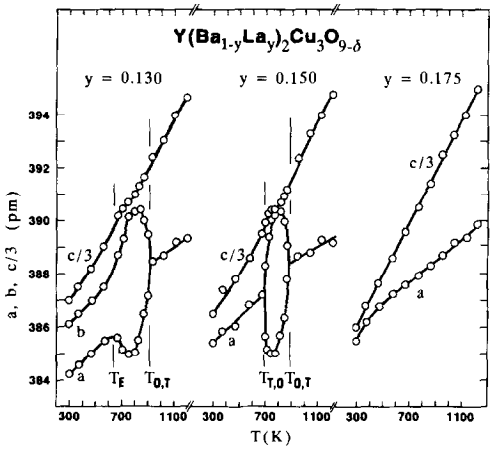

FIG. 6. Temperature variation of unit cell parameters of $Y(Ba_{1-y}La_y)_2Cu_3O_{9-\delta}$ between 300 and 1250 K in air, for $y = 0.13$, 0.15, and 0.175, $9 - \delta$ being 7.07, 7.11, and 7.15, respectively, prior to measurements. (Size of circles exceeds twice the calculated standard deviations; concerning T_E, $T_{O,T}$ and $T_{T,O}$, see text.)

the present data refer to equilibrium with the open atmosphere (P_{O_2} = 21 kPa). The temperature dependencies of the unit cell parameters for $y = 0.130$, 0.150, and 0.175 (Fig. 6) reflect two features: thermal expansion and thermal release of oxygen. The latter process takes place at a measurable rate above ~300°C.

As a consequence of the thermally induced removal of the additional oxygen, brought about by La, the orthorhombic distortion first increases, cf. the data for the $y = 0.130$ sample in Fig. 6. Upon further heating and oxygen depletion, the distortion vanishes, in analogy with the room temperature behavior of the getter-reduced samples, discussed above. Similarly, the initially tetragonal $Y(Ba_{0.85}La_{0.15})_2Cu_3O_{7.11}$ sample converts to orthorhombic at 360°C to revert back to tetragonal at 550°C. However, for $y = 0.175$, the absence of any line splitting or broadening in the high temperature PXD diagrams shows that there is no orthorhombic distortion between 20 and 920°C. The temperatures for the onset of enhanced orthorhombic distortion T_E and the tetragonal to orthorhombic transition $T_{T,O}$ are listed in Table II together with those for the "regular" orthorhombic to tetragonal transition $T_{O,T}$ (upon heating in air). While T_E (onset of oxygen release) is constant, the transition temperatures $T_{T,O}$ and $T_{O,T}$ gradually approach each other to merge at a point T = 630(50) K and y = 0.165(5), for constant p_{O_2} = 21 kPa. Above y = 0.165(5), the tetragonal structure prevails in air at all temperatures.

Discussion and Conclusions

The unit cell parameters of $Y(Ba_{1-y}La_y)_2Cu_3O_{9-\delta}$ respond significantly to La substitution ($y \in 0$, 0.36) and to the reversible oxygen change ($9 - \delta \in 6.0$, 7.3). A three-dimensional diagram showing the a and b unit cell parameters as functions of the La substitution y and the oxygen content $9 - \delta$ is presented in Fig. 7. Maximum orthorhombic distortion is found at zero substitution and close to $9 - \delta = 7$. For the substituted samples, the maximum orthorhombic distortion remains at oxygen contents between 6.90 and 7.00. The distortion dimin-

TABLE II

DISTORTION AND TRANSITION TEMPERATURES FOR $Y(Ba_{1-y}La_y)_2Cu_3O_{9-\delta}$

y	T_E	$T_{T,O}$	$T_{O,T}$
0.075	—	—	900
0.100	—	—	910
0.120	600	—	880
0.130	600	—	860
0.140	600	—	850
0.150	—	640	830
0.160	—	680	790
0.170	—	—	—

Note. As seen by high temperature PXD upon heating of oxygen-saturated samples in air; T_E, enhanced orthorhombic distortion; $T_{T,O}$, tetragonal to orthorhombic transition; $T_{O,T}$, orthorhombic to tetragonal transition; all in K.

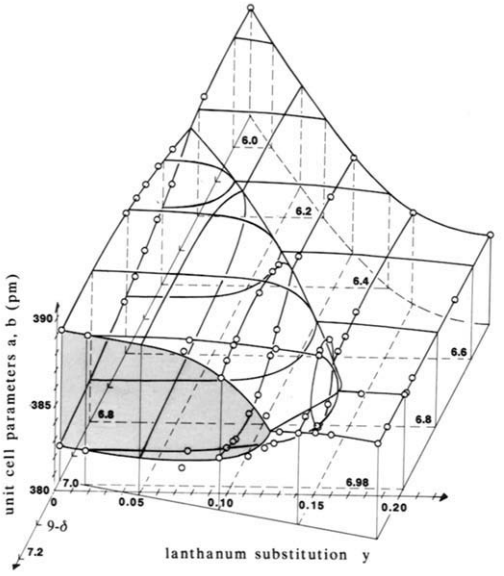

FIG. 7. Three-dimensional representation of unit cell parameters a and b (in pm) of $Y(Ba_{1-y}La_y)_2Cu_3O_{9-\delta}$ as a function of oxygen content $9 - \delta$ and La substitution y.

ishes for both lower and higher oxygen contents, as well as for increasing La content.

The structural consequences of an *oxygen content* below 6.90 to 7.00 follow from creation of vacancies at the O(1) site and, to a smaller extent, from a random filling of the O(5) site up to a point where the structure turns tetragonal. Accordingly, the unit cell parameters a and b, respectively, expand and contract faster upon oxygen removal than expected for a simple mixture of square (when $9 - \delta = 7$) and linear coordination (when $9 - \delta = 6$) of the Cu(1) atoms. Upon removal of the oxygen atoms, the shielding between the large positive charges at the neighboring Ba site diminishes and the structure expands in the direction of the c axis.

The structural consequences of an *oxygen content* above the 6.90 to 7.00 level follow from the accommodation of the additional oxygen atoms at the O(5) site.The proportion of octahedrally coordinated Cu(1) atoms then increases and, hence, the orthorhombic distortion decreases. In analogy with the situation when oxygen is removed, the structure becomes tetragonal before the O(5) site is completely filled.

The structural response to the *introduction of the smaller La atoms* can be derived from the structural behavior of the oxygen saturated samples provided a correction (based on Fig. 7) is made for the increased oxygen content. The anisotropic contraction implies an enhanced tendency toward tetragonal symmetry, as manifested both in site occupancies and atomic coordinates. Upon increasing substitution (see Table III), the O(3) and O(4) atoms approach the Ba/La site, but the Cu(2)–Cu(2) distance (across the Y site) remains at best constant. The whole of the c contraction is then realized along the Cu(1)–O(2)–Cu(2) bonds. The filling of the O(5) site at the expense of the O(1) site apparently provides a relaxation mechanism for the contraction, supported by the fact that no shrinkage occurs in the *ab* plane.

The implications of these substitution-induced changes in the structural properties on superconductivity are postponed to a

TABLE III

TRENDS IN INTERATOMIC DISTANCES FOR $Y(Ba_{1-y}La_y)_2Cu_3O_{6.91(2)}$

y: 0.075		0.100	0.150	0.200
Ba—O(1)	281.1(7)	280.6(7)	282.2(8)	284.4(8)
Ba—O(2)	272.4(2)	272.2(1)	272.4(2)	272.9(3)
Ba—O(3)	305.0(14)	304.6(14)	301.0(12)	297.4(13)
Ba—O(4)	300.4(13)	301.1(11)	301.0(12)	297.4(13)
Ba—O(5)	283.4(7)	282.3(7)	282.2(8)	284.4(8)
Cu(1)—O(1)	193.8(1)	193.4(1)	192.2(1)	192.2(1)
Cu(1)—O(2)	188.3(10)	188.2(9)	188.1(11)	185.1(13)
Cu(1)—O(5)	190.5(1)	191.0(1)	192.2(1)	192.2(1)
Cu(2)—O(2)	228.1(16)	226.5(13)	223.1(18)	225.4(20)
Cu(2)—O(3)	192.2(3)	192.8(2)	194.1(2)	194.0(2)
Cu(2)—O(4)	195.1(2)	194.9(2)	194.1(2)	194.0(2)
Cu(2)—Cu(2)	327.4(12)	329.9(10)	333.3(15)	332.7(15)
Y—O(3)	237.8(6)	238.1(6)	237.5(4)	238.0(4)
Y—O(4)	237.0(5)	237.7(6)	237.5(4)	238.0(4)

Note. Distances (in pm, at 8 K) are calculated according to Table I. Labeling of atoms for $y = 0.150$ and 0.200 is orthorhombic as for $y = 0.075$ and 0.100.

more detailed analysis in a separate communication (*33*).

Acknowledgments

This work received financial support from the Norwegian Council for Science and the Humanities (NAVF).

References

1. J. G. Bednorz and K. A. Müller, *Z. Phys. B* **64,** 189 (1986).
2. P. Strobel, J. J. Capponi, M. Marezio, and P. Monod, *Solid State Commun.* **64,** 513 (1987).
3. A. W. Hewat, J. J. Capponi, C. Chaillout, M. Marezio, and E. A. Hewat, *Solid State Commun.* **64,** 301 (1987).
4. C. C. Torardi, E. M. McCarron, P. E. Bierstedt, A. W. Sleight, and D. E. Cox, *Solid State Commun.* **64,** 497 (1987).
5. E. Kaldis, P. Fischer, A. W. Hewat, E. A. Hewat, J. Karpinski, and S. Rusiecki, *Physica C (Amsterdam)* **159,** 668 (1989).
6. J. B. Goodenough, A. Manthiram, Y. Dai, and A. Campion, *Supercond. Sci. Technol.* **1,** 187 (1988).
7. A. F. Andresen, H. Fjellvåg, P. Karen, and A. Kjekshus, *Z. Kristallogr.* **185,** A2 (1988).
8. R. J. Cava, B. Batlog, R. M. Fleming, S. A. Sunshine, A. Ramirez, E. A. Rietman, S. M. Zahurak, and R. B. von Dover, *Phys. Rev. B: Condens. Matter* **37,** 5912 (1988).
9. T. C. Huang, Y. Yokura, J. B. Torrance, A. I. Nazzal, and J. Karimi, *Appl. Phys. Lett.* **52,** 1901 (1988).
10. A. Suzuki, E. V. Sampathkumaran, K. Kohn, T. Shibua, A. Tohdake, and M. Ishikawa, *Jpn. J. Appl. Phys., Part 2* **27,**L797 (1988).
11. A. Tokiwa, Y. Syono, M. Kikuchi, R. Suzuki, T. Kajitani, N. Kobyashi, T. Sasaki, O. Nakatsu, and Y. Muto, *Jpn. J. Appl. Phys., Part 2* **27,** L1009 (1988).
12. A. Manthiram, X. X. Tang, and J. B. Goodenough, *Phys. Rev. B: Condens. Matter* **37,** 3734 (1988).
13. P. A. J. DeGroot, G. P. Rapson, B. D. Rainfort, M. T. Weller, J. R. Grasmeder, and P. C. Lancester, *Physica C (Amsterdam)* **152,** 483 (1988).
14. S. Mazumder, H. Rajagopal, A. Sequeira, R. Venkatramani, S. P. Garg, A. K. Rajarajan, L. C. Gupta, and R. Vijayaraghavan, *J. Phys. C: Solid State Phys.* **21,** 5967 (1988).
15. A. Sequeira, H. Rajagopal, S. Mazumder, A. K. Rajarajan, P. Ayyub, L. C. Gupta, and R. Vijayaraghavan, *Rev. Solid State Sci.* **2,** 229 (1988).
16. R. Liang, M. Itoh, T. Nakamura, and R. Aoki, *Physica C (Amsterdam)* **157,** 83 (1989).
17. M. R. Chandrachood, I. S. Mulla, and A. P. B. Sinha, *Solid State Commun.* **68,** 1005 (1988).
18. D. E. Morris, P. Narwankar, A. P. B. Sinha, K. Takano, and T. Shum, Lawrence Berkeley Laboratory (1990). [Preprint]
19. P. E. Werner, "The Computer Programme SCANPI," Institute of Inorganic Chemistry, University of Stockholm, Sweden (1981).
20. N. O. Ersson, "Programme CELLKANT," Chemical Institute, Uppsala University, Uppsala, Sweden (1981).
21. H. M. Rietveld, *J. Appl. Crystallogr.* **1,** 65 (1968).
22. A. W. Hewat, *UKAERE Harwell Rep.* RRL 73/897 (1973).
23. L. Koester, and W. B. Yelon, *in* "Neutron Diffraction Newsletter," (W. B. Yelon, Ed.) The Neutron Diffraction Commission, MO (1983).
24. P. Karen, H. Fjellvåg, O. Braaten, A. Kjekshus, and H. Bratsberg, *Acta Chem. Scand.* **44,** 994 (1990).
25. D. M.De Leeuw, *J. Less-Common. Met.* **150,** 95 (1989).
26. H. Fjellvåg, P. Karen, and A. Kjekshus, *Acta Chem. Scand. A* **41,** 283 (1987).
27. P. Karen, O. Braaten, H. Fjellvåg, and A. Kjekshus, "Proc. AMSAHTS '90," NASA Conf. Publ. 3100, Greenbelt, MD (1990) p. 117.
28. H. M. O'Bryan, and P. K. Gallagher, *Solid State Ionics* **32,** 1143 (1989).
29. R. J. Cava, B. Batlogg, K. M. Rabe, E. A. Rietman, P. K. Gallagher, and L. W. Rupp, Jr., *Physica C (Amsterdam)* **156,** 523 (1988).
30. S. Nakanishi, M. Kogachi, H. Sasakura, N. Fukuoka, S. Minamigava, K. Nakahigashi, and A. Yanase, *Jpn. J. Appl. Phys., Part 2* **27,** L329 (1988).
31. R. J. Cava, A. W. Hewat, E. A. Hewat, B. Batlogg, M. Marezio, K. M. Rabe, J. J. Krajewski, W. F. Peck Jr., and L. W. Rupp Jr., *Physica C (Amsterdam)* **165,** 419 (1990).
32. T. Graf, T. Triscone, and J. Muller, *J. Less-Common Met.* **159,** 349 (1990).
33. P. Karen, H. Fjellvåg, and A. Kjekshus, to be submitted.